Effects of magnification and sampling resolution in X-ray computed tomography for the measurement of additively manufactured metal surfaces

Adam Thompson[1], Nicola Senin[1,2], Ian Maskery[3], Richard Leach[1]
[1]Manufacturing Metrology Team, University of Nottingham, Nottingham, NG7 2RD, UK
[2]Department of Engineering, University of Perugia, 06125, Italy
[3]Centre for Additive Manufacturing, University of Nottingham, Nottingham, NG7 2RD, UK

Abstract. Recent studies have shown that X-ray computed tomography (XCT) can be used to measure the surface topography of additively manufactured parts. However, further research is necessary to fully understand XCT measurement performance. Here, we show how magnification of the X-ray projections and resolution of the volumetric reconstruction grid influence the determination of surface topography in the XCT data processing pipeline. We also compare XCT results to coherence scanning interferometry (CSI) measurements and find that by increasing the magnification of the X-ray projections, smaller topographic detail can be resolved, approaching the lateral resolution of CSI. Results show that there is an optimum setting for magnification, below and above which XCT measurement performance can degrade. The resolution of the volumetric reconstruction grid has a less pronounced effect, but in general, adopting higher or lower resolutions than the default leads to degraded repeatability in surface determination. The problem of determining sensitivity of XCT surface measurement as a function of setup parameters is complex, and it is not yet possible to provide optimal setup configurations that work regardless of object geometry. However, the methods presented here, as well as the results obtained, represent a useful contribution to good practice for XCT measurement of surfaces.

Key words: X-ray computed tomography, metrology, surface texture, metal powder bed fusion

1. Introduction

Additive manufacturing (AM) represents a new technique in the toolbox of production processes, in that the design freedom provided by AM enables the creation of parts that have not previously been possible using conventional subtractive manufacturing methods [1]. For example, many AM processes are capable of producing freeform hollow, trabecular or otherwise complex and topologically optimised parts, capable of significant mass saving in high-value applications, such as in the aerospace, automotive and biomedical sectors.

There are currently a number of substantial barriers to increased adoption of AM technologies. If a manufacturer wishes to place a part into a commercial aircraft, for example, rigorous verification standards must be met in order to ensure the sufficiency of that part's quality. However, when compared to parts produced by conventional means, additive manufacturers encounter issues relating to poor mechanical performance (for example, fatigue [2], creep [3]), limitations in the pool of available materials, and difficulty in verification of parts [4,5].

Existing part inspection and verification practices are well developed, and work well for conventionally manufactured parts, but AM parts commonly cause additional issues. Conventional verification methods involving co-ordinate measuring systems are often not possible [6], as the geometries commonly produced by AM processes contain features inaccessible to conventional measurement technologies. In particular, AM parts commonly contain function-critical surfaces that are inaccessible to both contact and optical measurement technologies [7].

To overcome the issues faced by contact and optical measurement technologies, X-ray computed tomography (XCT) has been increasingly recognised as a viable solution for dimensional measurements in AM [8]. Similarly to AM technologies, however, a relatively poor understanding of the XCT measurement process is one of the factors preventing more widespread industrial adoption, and substantial work is required to qualify XCT as a reliable verification method [9]. Particularly, XCT has become recognised in a number of recent publications [7,10–15] as a viable method of surface topography measurement for internal and hard-to-reach surfaces. Pyka et al. [10,11] made the first XCT surface measurements, in which they extracted profiles from XCT orthoslices and computed ISO 4287 [16] texture parameters on these profiles. Thompson et al. [7,13,17] and Townsend et al. [14,15] later extracted areal topographies from XCT data and compared them to data acquired using state-of-the-art optical surface measurement technologies. Townsend et al. [14] compared XCT surface data to focus variation [18,19] measurements by examining ISO 25178-2 [20] areal texture field parameters. They examined how a number of factors affect XCT surface measurements [15], focusing on surface determination methods, XCT filament replacement and internal against external surface measurement. In recent work [13,17], we presented the results of a comprehensive effort involving the direct quantification of discrepancies between topographic reconstructions, covering XCT surface measurement in comparison to the major optical areal topography measurement technologies: confocal microscopy [21,22], coherence scanning interferometry (CSI) [23,24] and focus variation microscopy [18,19]. We also found during the aforementioned studies that the surface topographies produced by XCT measurement can be highly variable (see figure 1) depending on the setup of the measurement parameters in the instrument.

A comprehensive assessment of XCT performance and behaviour when measuring surface topography, as well as a thorough exploration of the effects of the numerous involved measurement process parameters, has yet to be performed. The challenge represented by this assessment is significant, because of the large number of variables involved in the initial acquisition of the X-ray projections, in their combination into a volumetric dataset, and in the final extraction of surface topography [7].

Here, we investigate the effects of changing two variables during the measurement process. The first of which is one of the most important parameters set during X-ray image acquisition: the magnification of the X-ray projections. Referred to as *magnification* in the following, this is the ratio between the X-ray source-to-detector distance and the X-ray source-to-object distance [25] (see figure 2a). The latter variable is one of the most important variables set during volumetric reconstruction: the resolution of the volumetric reconstruction grid [26] (see figure 2b); referred to hereafter as *resolution*. Both magnification and reconstruction affect the capability of the instrument to resolve small topographic detail in the extracted surface. For this experiment, we use a cone beam XCT system, circular scanning and a planar detector. Volumetric reconstruction is performed using the manufacturer's implementation of the Feldkamp, Davis and Kress (FDK) algorithm [27]. As such, our results reflect this general setup.

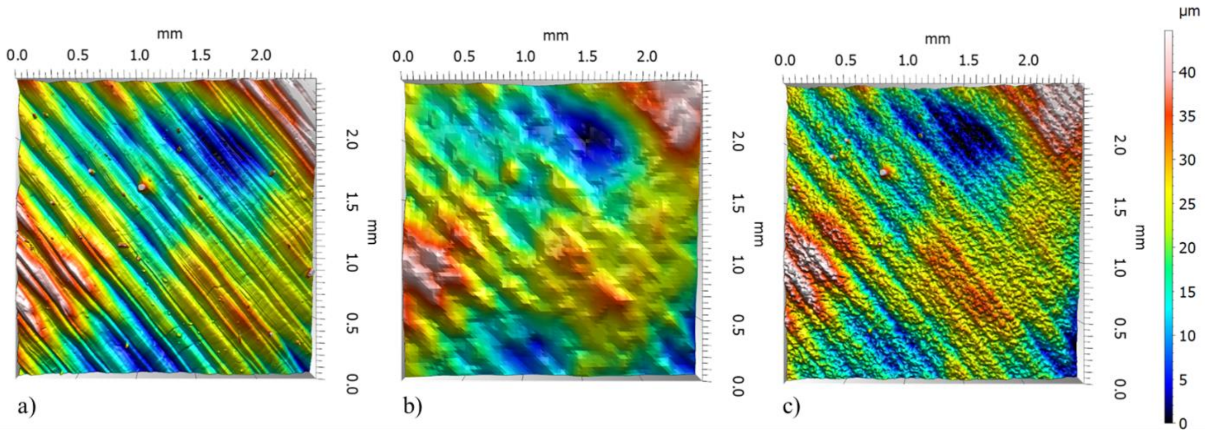

Figure 1. Example topographies obtained by varying XCT measurement setup: a) CSI reference; b) XCT measurement using 5× magnification; c) XCT measurement using 20× magnification.

2. Methods

2.1 Sample

The test sample, developed to study internal surfaces in previous work [7], was comprised of two separable halves that could be combined to form a hollow cube of size (10 × 10 × 10) mm. The sample was fabricated using an EOSINT M 280 metal LPBF machine in Ti6Al4V. The test surface chosen was a nominally flat top surface, i.e. the final surface built in the LPBF machine, in the plane orthogonal to the build direction. X-ray images (i.e. projections) were taken, at different magnifications (5×, 10×, 20× and 50×). Each set of projections was used for multiple volumetric reconstructions using resolutions: 50 %, 100 % and 150 %, where 100 % corresponds to the resolution of the detector. For example, in the 20× magnification, 100 % resolution case, a detector containing a grid of 2000 × 2000 pixels of size (0.2 × 0.2) mm will yield a reconstructed volume containing 2000 × 2000 × 2000 voxels, each of size (10 × 10 × 10) µm. The 50 % and 150 % cases will then contain 1000 × 1000 × 1000 voxels, each of size (20 × 20 × 20) µm, and 3000 × 3000 × 3000 voxels, each of size (6.7 × 6.7 × 6.7) µm, respectively (see figure 2b). The 150 % and 50 % cases are examples of super-sampling and sub-sampling conditions, respectively.

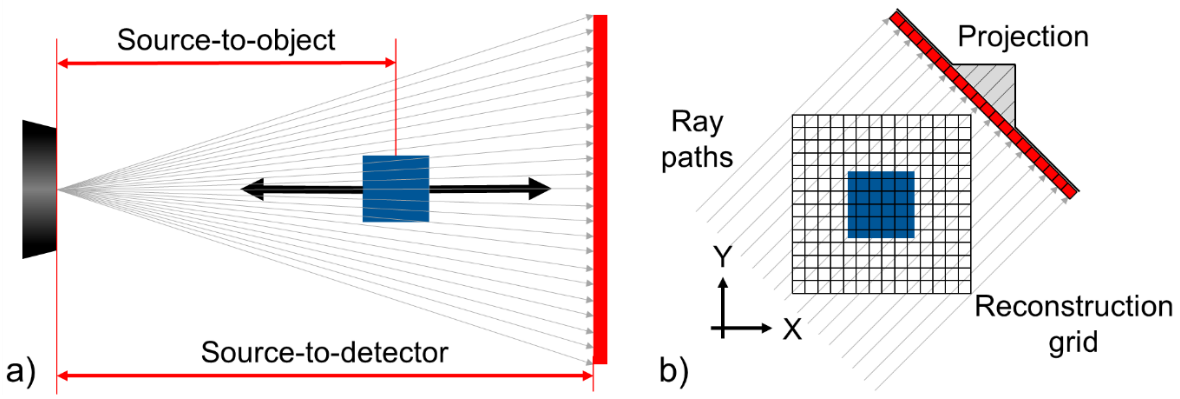

Figure 2. Investigated variables: a) geometric magnification in scanning; b) volumetric grid resolution in reconstruction by filtered back projection, representing the 100 % case [26].

2.2 Measurement setups

The sample was measured using a number of XCT measurement setups, as well as by CSI. In all measurement setups, five repeat measurements were taken in sequence, on the same instrument, with the same operator and without moving the sample between acquisitions.

XCT measurements were performed using a Nikon MCT 225, at geometric magnifications of 5×, 10×, 20× and 50×. The following parameters were used in all XCT measurement setups: voltage 200 kV, current 49 µA, 3142 projections, exposure 2000 ms and gain 24 dB. A detector shading correction was applied by averaging 512 reference frames (256 bright and 256 dark) and a warmup scan of approximately one hour was performed prior to scans. A 0.5 mm copper pre-filter was used between the X-ray source and the specimen. All measurements were set up in such a way that image resolution was limited by detector pixel size as opposed to the focal spot, in order to neglect the influence of the focal spot size on measurement data. X-ray imaging and volumetric reconstruction were performed using manufacturer's proprietary software (X-Inspect and CT-Pro, respectively), using the FDK algorithm [27] with a second order beam hardening correction and a Hanning noise filter, with cut-off at the maximum spatial frequency. This filter was chosen to reduce image noise present when alternatively using an edge-preserving ramp filter, without substantially degrading the quality of the edges present in the data. Noise was an issue in certain measurement setups, but application of a stronger noise filter would have caused unacceptable degradation of edges [28]. Super- and sub-sampling of the reconstruction grid was performed using CT Pro, creating twelve measurement setups in total. The voxel sizes resulting from each measurement setup are presented in table 1.

Table 1. Voxel size for each XCT setup/µm.

Magnification / Sampling resolution	5×	10×	20×	50×
50 %	80.0	40.0	20.0	8.0
100 %	40.0	20.0	10.0	4.0
150 %	26.7	13.3	6.7	2.7

CSI measurements were performed using a Zygo NewView 8300 in the following setup: 20× objective lens at 1× zoom, NA 0.40, FOV (0.42 × 0.42) mm, LR-pixel 0.41 µm, LR-optical 0.68 µm, where FOV is the field of view and LR is lateral resolution. LR-pixel refers to the pixel width of the detector and LR-optical refers the calculated Sparrow optical limit. During analysis, one CSI measurement was noted to have experienced unexpected data dropout across a portion of the measurement area, resulting in outliers in the calculation of ISO 25178-2 [20] texture parameters. This dataset was removed from the study and data comparison was performed using the remaining four repetitions (see also supplementary information). Regarding the uncertainty of the CSI system, the instrument manufacturer quotes surface topography repeatability of 0.12 nm, step height repeatability of 0.1 % and step height accuracy of 0.3 % [29]. When measuring very rough surfaces, the absolute accuracy of surface topography measurement and topography repeatability are complex to evaluate, and the subject of current significant research efforts (e.g. see [30]). In recent comparable studies, CSI systems have been shown capable of measuring metal AM surfaces to good quality levels [31] and so a CSI instrument is used here as a reference.

2.3 Data analysis

Following reconstruction, XCT data were imported into Volume Graphics VGStudioMAX 3.0 [32] and surfaces were determined using the local maximum gradient algorithm over a search distance of four voxels, using the ISO 50 % isosurface [33] as the start point. For the three 50× datasets, an additional opening/closing [34] operation was performed to remove noise artefacts from the surface. The computed surfaces were exported as triangulated meshes in the STL format with no mesh simplification. Surfaces were then imported into MountainsMap [35], where they were automatically converted into 2.5D digital elevation models (DEMs) to allow comparison to CSI data. DEMs are representations of height points on a grid commonly used in surface measurement, also known as 'height maps'. DEM resolutions were automatically determined by MountainsMap to match the point density of the triangulated meshes. The conversion removed any undercut features from the XCT data.

DEMs were imported into an in-house developed MATLAB [36] program, where they were converted into triangulated meshes for alignment in six degrees of freedom. Alignment was performed using a two-step algorithmic procedure: coarse alignment by distance minimisation of matched landmarks (visual identification of landmarks and application of the Procrustes method [37]), and fine alignment by application of the ICP method [38] using the sum of squared distances between paired points as the minimisation objective (global alignment). Topographies generated using the XCT 5×/50 % setup had insufficient topographic detail to allow alignment, so were not considered in the analysis. A single CSI dataset was taken as the global alignment reference, and one XCT dataset for every combination of magnification and resolution was aligned to it. Other replicates in each XCT setup were then aligned to the first one of each set. As the alignment took place in six degrees of freedom, all the aligned datasets were finally reconverted into height maps by application of a custom *z*-ray tracing algorithm that performs an *xy* raster scan of the triangulated mesh (implemented in MATLAB). The *xy* raster scanning grid was set at 5 µm spacing. Although greater than the point spacing in some of the original CSI and XCT datasets, this 5 µm spacing was chosen as a compromise between the need to minimise information loss and the need to prevent excessive computation time in higher resolution data. ISO 25178-2 [20] texture parameters were calculated in MountainsMap, while statistical modelling of topographies was performed in MATLAB. For calculation of texture parameters, a levelling F-operator (removal of a least-squares mean plane) was applied. No L- or S-filters were applied so as to maximise the measurement bandwidth, as data are intrinsically bandwidth matched [39] during the alignment, cropping (matching of larger wavelengths) and raster scanning (matching of smaller wavelengths) process. This bandwidth matching process homogenises the range of spatial frequencies across all data, preventing differences in calculated parameters as a result of spatial frequencies present in some datasets and not others (i.e. accounting also for partial volume effects, typically causing the loss of higher spatial frequencies in lower magnification data [9]).

3. Results

3.1 Projections and orthoslices

Example projections at each magnification are shown in figure 3 (top). An initial analysis of the reconstructed volumetric datasets, performed via visual inspection of digital slices extracted from the datasets (orthoslices), showed an increasing, irregular dispersion of intensity values at higher magnifications, as observable in the middle and lower parts of figure 3. The bottom images of figure 3 also show the dependency of image sharpness on magnification.

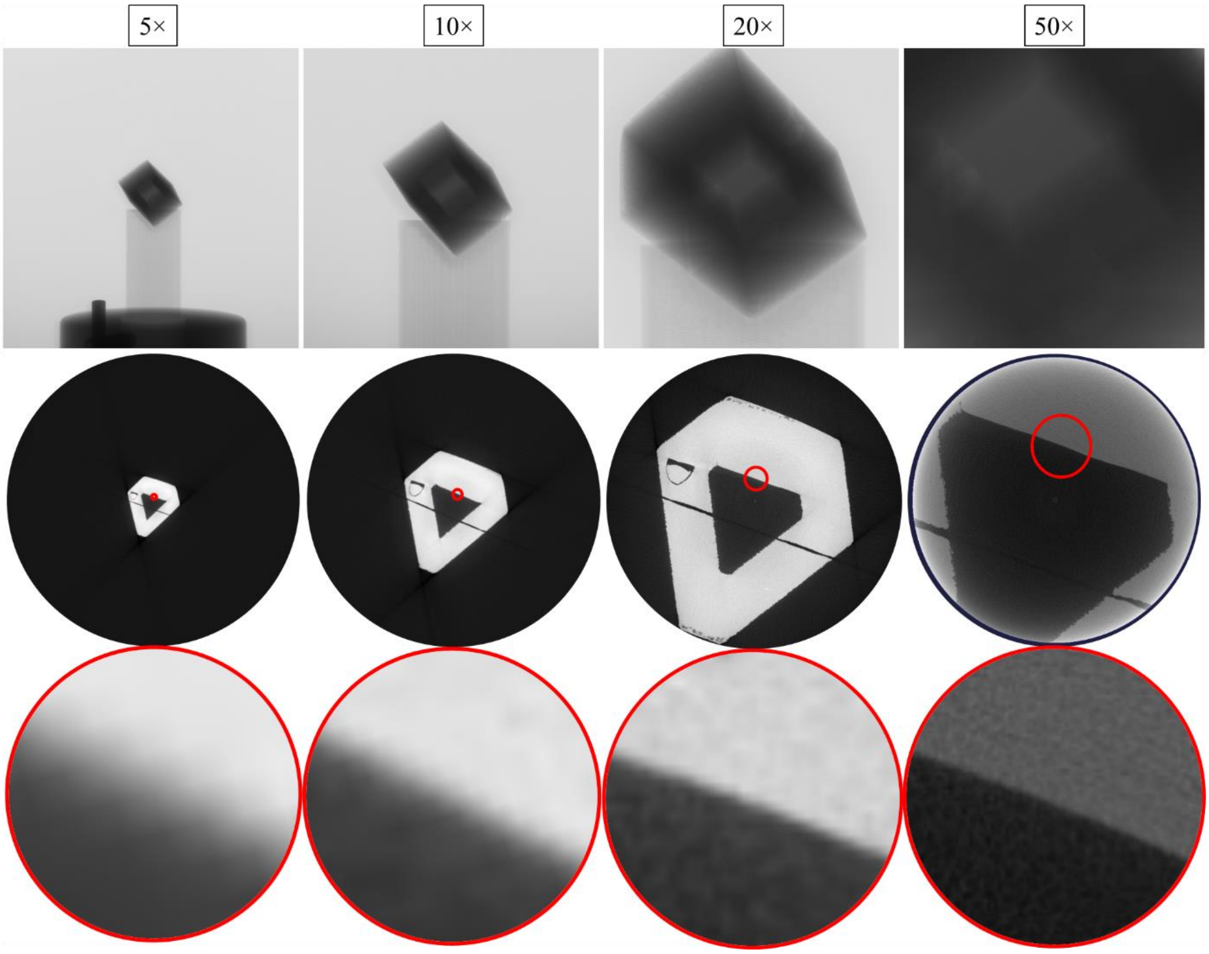

Figure 3. Magnification and its effects on projections and volumetric reconstruction; top: example individual projections obtained at increasing magnifications; middle: orthoslices (i.e. perpendicular to the rotation axis) extracted from the final volumes obtained at the same geometric magnifications, using 100 % resolution in the volumetric reconstruction step; bottom: magnified portions of orthoslices highlighted with red rings in middle images.

3.2 Topography preparation and comparison via texture parameters

XCT surface topographies were obtained by extracting surfaces from the volumetric datasets generated by all the combinations of magnification and resolution, repeating the measurement process on the same volume in each setup five times. Repeat measurements were taken under repeatability conditions; in that the same operator performed the measurement in sequence on the same instrument, without removing the sample. Further topography datasets were obtained using repeat CSI measurement of the same surface region. Visualisations of all datasets (similar to those displayed in figure 1) are available as supplementary information. CSI measurement was chosen as a reference, having previously been identified as an effective technology for measuring metal additive surfaces [31]. Although establishing traceability [40] for data acquired using a CSI system has not yet been undertaken for such complex samples (see section 3.1), the CSI can in this case be considered as a sufficient reference when compared to XCT, which exhibits substantially poorer accuracy and precision by comparison [17]. CSI setup parameters were chosen in accordance with previously published research on CSI measurement [31]. Topography datasets were aligned in space using the method presented in the work of Senin et al. [13] and cropped to the same region of interest to prevent discrepancies caused by topographic features present only in some datasets (for example, peaks or pits that would fall outside the field of view in some measurements). Several ISO 25178-2 areal texture field parameters [20] were computed to quantify topographic properties. Specifically the parameters used were: *Sa*, the arithmetical mean absolute deviation of heights from the mean plane; *Sq*, the root mean square deviation of heights from the mean plane; *Ssk*, the skewness of the height distribution – essentially, the degree of asymmetry of the probability distribution of heights; Sku, the kurtosis of the height distribution – essentially, how similar the probability distribution of heights is to a Gaussian; *Sdr*, the developed area ratio – the ratio between the actual area of the surface and the projected area on the *xy* plane; Sal, the autocorrelation length – the length to which the surface is sufficiently self-similar and *Sdq*, the root mean square gradient of the surface. Further information on the selected texture parameters, as well are more complete definitions, can be found in the standard ISO 25178-2 [20]. Confidence intervals (at 95 % confidence) on their means within the repeat measurements were used to investigate differences between measurement setups. The results of this analysis are displayed in figure 4.

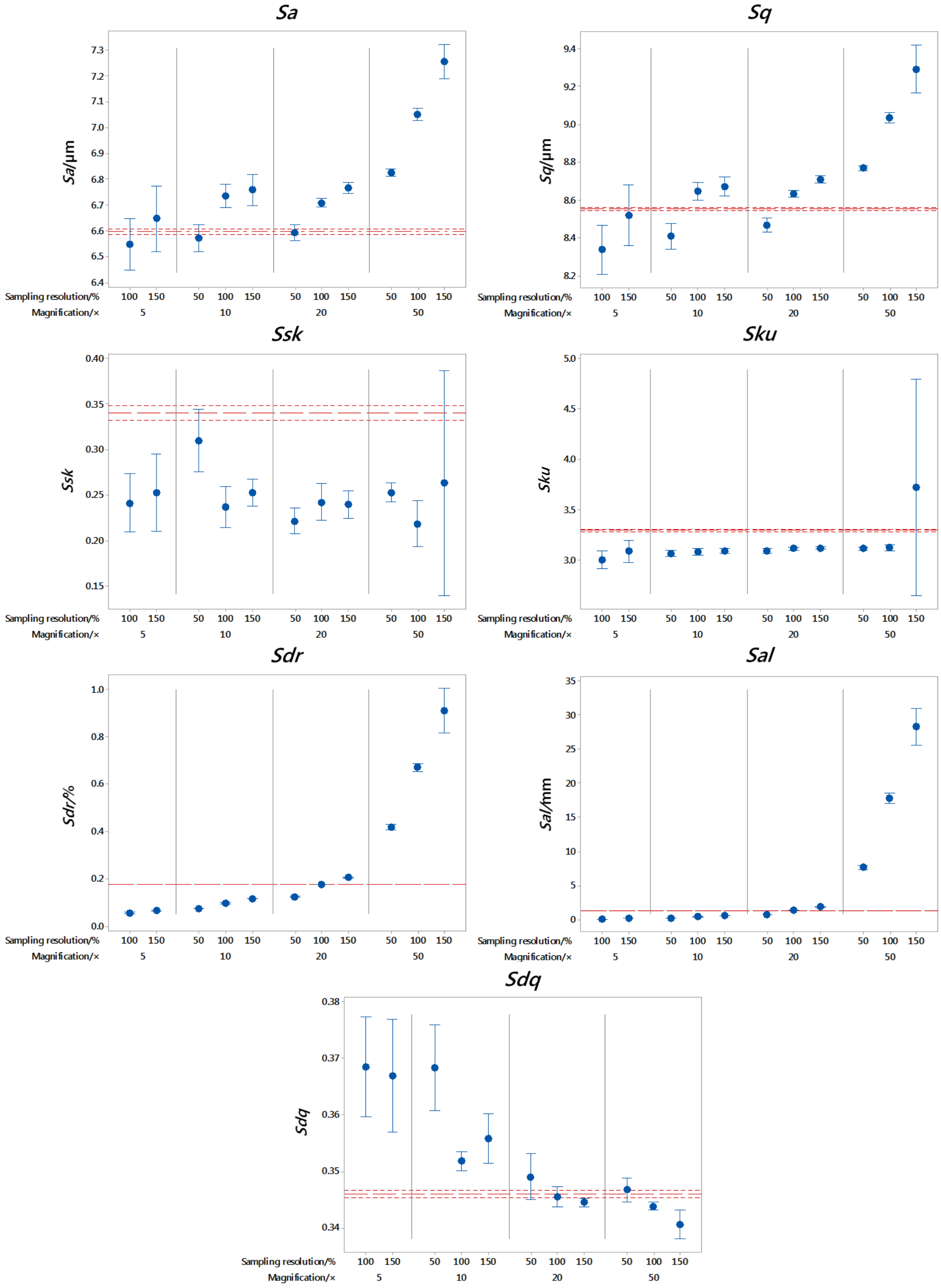

Figure 4. ISO 25178-2 [20] areal texture field parameters computed for each XCT measurement setup (magnification and sampling resolution) and compared to the results for the CSI datasets (represented as reference lines, where the coarse dashed lines are means and fine dashed lines are the upper and lower

CI bounds). The 5×/50 % setup is omitted as the topography of the reconstructed XCT surface was too deprived of detail to allow accurate alignment to CSI data. Confidence intervals computed at 95 % confidence on the repeat measurements.

3.3 Comparison via statistical topography models

Areal texture field parameters are essentially statistical descriptors, i.e. they are designed to summarise complex topographical properties pertaining to an entire surface region using scalar values. In figure 4, discrepancies can be seen between XCT and CSI parameters, for example, *Ssk* and *Sku* parameters are routinely underestimated by XCT setups compared to CSI, and the 50×/150 % setup has here resulted in much larger CIs for these parameters than other setups. Discrepancies between texture parameter values imply the existence of topographical differences, but can provide only limited information on their exact nature, shape and spatial distribution. Therefore, to investigate topographical differences resulting from different XCT magnifications and resolutions, we adopted a method developed in our previous work [13,17]. This method involves the generation of statistical topographic models based on the same repeat measurements used for computing areal texture parameters. With reference to figure 5, each statistical model referring to a specific XCT setup (magnification and sampling resolution) is comprised of a mean surface and confidence intervals (CIs) on the local mean height. These CIs – interpolated over the surface – create an upper and lower confidence boundary which identifies the estimated location of the mean height at a given confidence level (95 % in this test case). As in our previous work [13,17], here, CIs were obtained by treating the heights collected at each (x,y) location as independent random variables (i.e. without modelling spatial correlation between surface points) and by using t-distributions to estimate the CIs. Statistical topography models built for each XCT setup were used to assess local repeatability error (identified by the local width of the CIs) as a consequence of the setup choice. Statistical models were compared in pairs and used to assess disagreements between local mean height values. Upper and lower surfaces obtained by interpolation of the extreme points of the local CIs are displayed in figure 6 (for all combinations of magnification and resolution). In each case shown in figure 6, upper and lower bounds for the reference CSI dataset are also rendered.

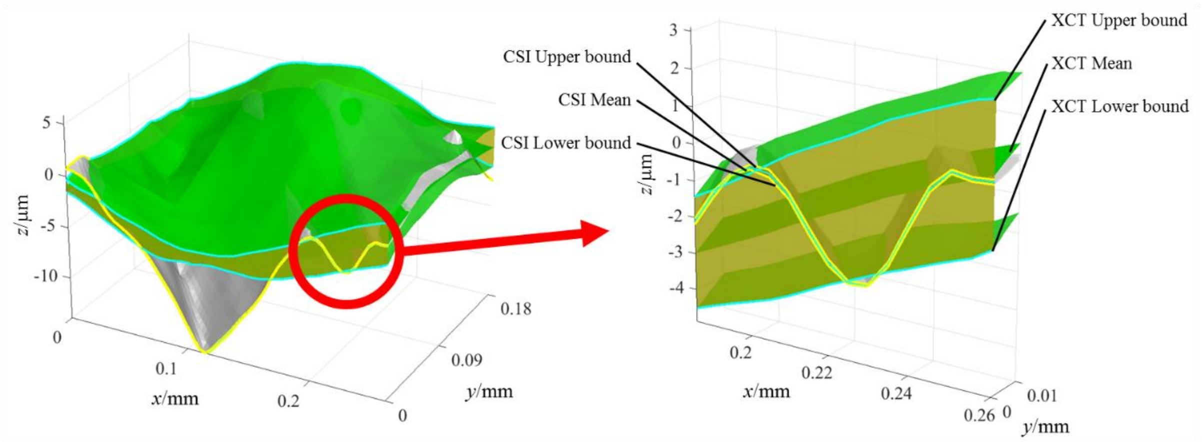

Figure 5. Statistical topography models, showing XCT and CSI mean surfaces and upper and lower bounds (extreme points of local CIs).

Figure 6 shows that as magnification and sampling resolution increase, the topographic detail in the reconstructed surface improves. However, as magnification increases, the dispersion of height values across replicate measurements also increases (i.e. the CI widths get larger and more irregular), indicating larger repeatability error. At 50×, the dispersion of height values essentially compromises the beneficial effects achieved in terms of better topographic detail.

Statistical models were also used to assess local discrepancy between mean height values estimated by each measurement setup. In these models, regions where CIs do not overlap can be considered as regions where the difference between heights is statistically significant. Using this information, we then defined a measure of overall discrepancy between measurement setups, computed as the ratio between the total area of the regions where height differences are statistically significant, over the total measured area. By pairing datasets acquired using each XCT setup to the CSI dataset, we can interpret any region where height difference is statistically significant as a region where local bias in the XCT measurement can be detected with 95 % confidence; thus obtaining an indication of the measurement accuracy of each XCT setup.

Local bias of the XCT measurements, with respect to the CSI reference is also shown in Figure 6. For XCT setups where repeatability error is lower (i.e. narrower CIs), discrepant regions are visible across the field of view. However, for XCT setups where the repeatability error is larger, discrepant regions are less common. This decrease in discrepancy does not necessarily mean that the agreement between measurements has improved, but rather that a higher number of repeat measurements is needed to better assess the statistical significance of the discrepancies.

In figure 7, the previous results are reorganised to provide another perspective to our findings. Particularly, the mean width of CIs computed over the sample region is shown as a function of magnification and resolution as a surface function, obtained by bilinear interpolation between experimental data points. The mean width of the CIs should be interpreted as a mean repeatability error for a given setup. Results show that the mean repeatability error is at minimum in the 20× data, but increases at lower or higher magnifications. Modification of the sampling resolution also has an effect, with repeatability error worsening at increased sampling rates.

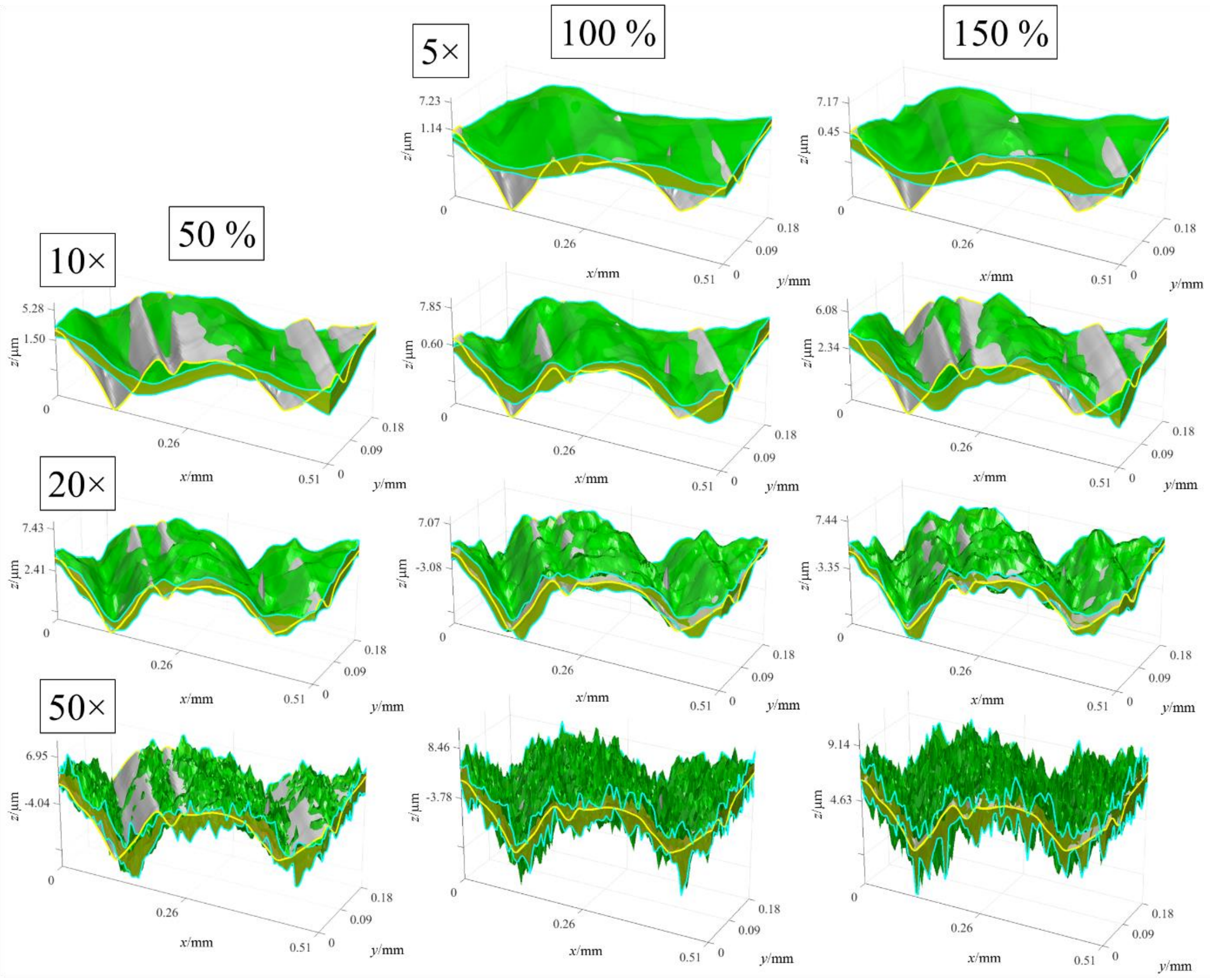

Figure 6. Statistical topography models for each XCT setup, compared to the CSI setup. The 5×/50 % setup is omitted as the topographical detail of the reconstructed XCT surface was too deprived of topographical detail to allow accurate alignment to CSI data.

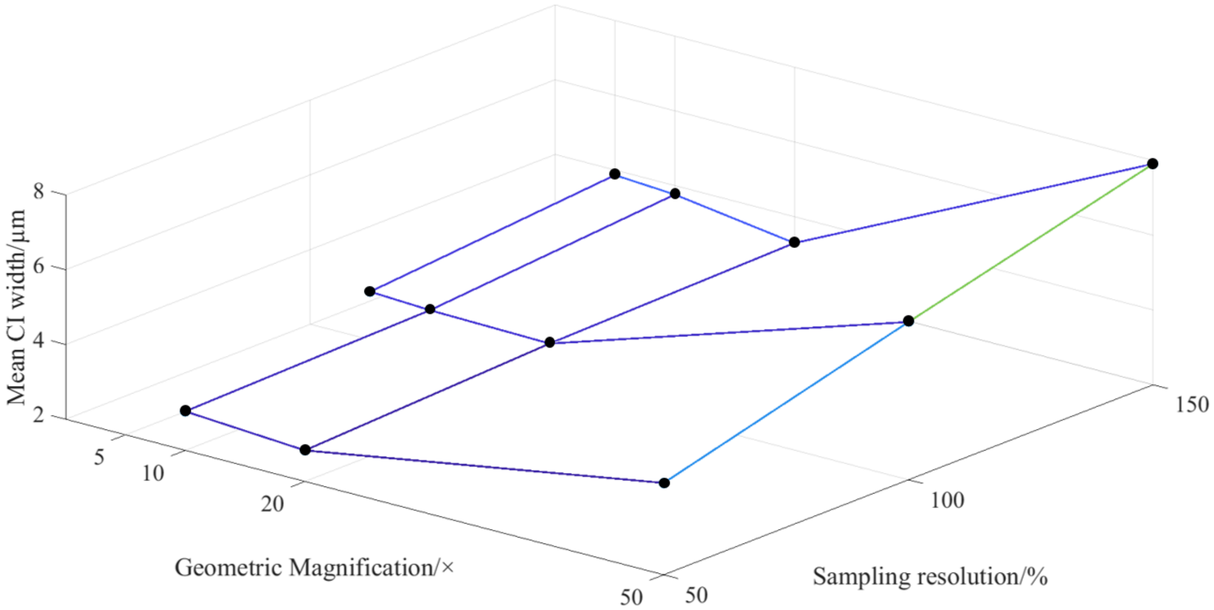

Figure 7. Mean repeatability error of XCT measurement corresponding to each setup, shown as an interpolated surface function. The mean repeatability error is computed as the arithmetic average of the CI widths over the sample region. The 5×/50 % setup is omitted as the topographical detail of the reconstructed XCT surface was too deprived of topographical detail to allow accurate alignment to CSI data.

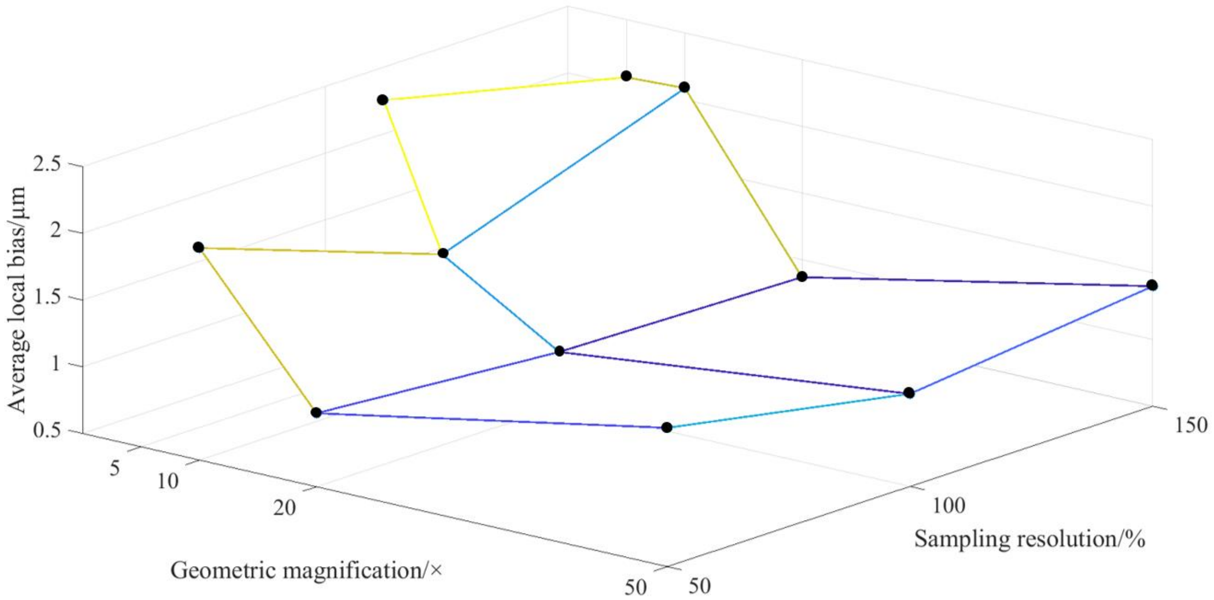

Figure 8. Arithmetic average of local bias in height determination when comparing each XCT measurement setup to CSI shown as interpolated surface function. The 5×/50 % setup is omitted as the topographical detail of the reconstructed XCT surface was too deprived of topographical detail to allow accurate alignment to CSI data.

In figure 8, the mean surface obtained for each XCT setup is compared to the mean CSI surface, corresponding to the same (x,y) positions. The arithmetic average of the local unsigned difference between means was elected as a measure of mean bias (accuracy) of the XCT measurement with respect to the CSI reference. In figure 8, the results are shown as a surface function (bilinear interpolation between experimental data points). The relationship between magnification, sampling resolution and the resulting accuracy shows the existence of a local minimum, corresponding to the 20×/150 % sampling resolution setup (i.e. least mean bias with respect to the CSI reference).

3.4 Comparison between paired, single surface datasets

In addition to comparing mean surfaces and the upper/lower bounds of statistical topography models, it is also possible to gain useful information by comparing paired, individual observations (i.e. individual topography datasets); as explained diagrammatically in figure 9, whilst all the combinations of paired comparisons are reported in figure 10. Each plot represents a specific XCT surface (green) aligned to the same CSI dataset (grey). Local distances are coloured proportionally to signed differences between height values. The increase of local topographic detail in the XCT datasets as magnification and resolution increases is even more evident in this figure than in figure 6, because of the absence of the smoothing effect introduced in the upper, mean and lower surfaces by the statistical model. An increase in high-spatial frequency, seemingly random, topographic content is also visible, most notably relating to magnification. This is the topographic component primarily responsible for the irregular behaviour of the local mean and corresponding upper/lower bounds observed in the statistical models corresponding to higher magnification presented in figure 6.

Further inspection of figures 6 and 8 indicates that, in any XCT setup, both local bias and repeatability error seem to be related to local topographic properties. This relation implies that it is likely that specific topographic features may trigger specific variations in measurement behaviour, sometimes mostly influencing bias, other times mostly influencing repeatability error. As such, the process of performing an uncertainty analysis for XCT surface measurement would be complex and difficult to apply generally, and a requirement for a task specific analysis is likely. Significant further investigation is therefore required into the significance of this problem and how it may be potentially minimised.

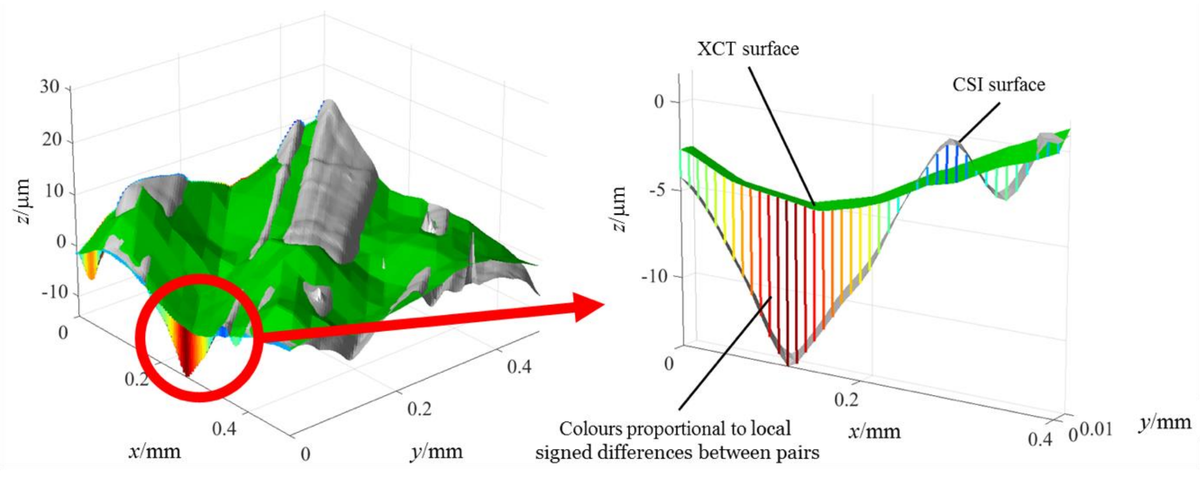

Figure 9. Local height differences (signed) computed between paired datasets.

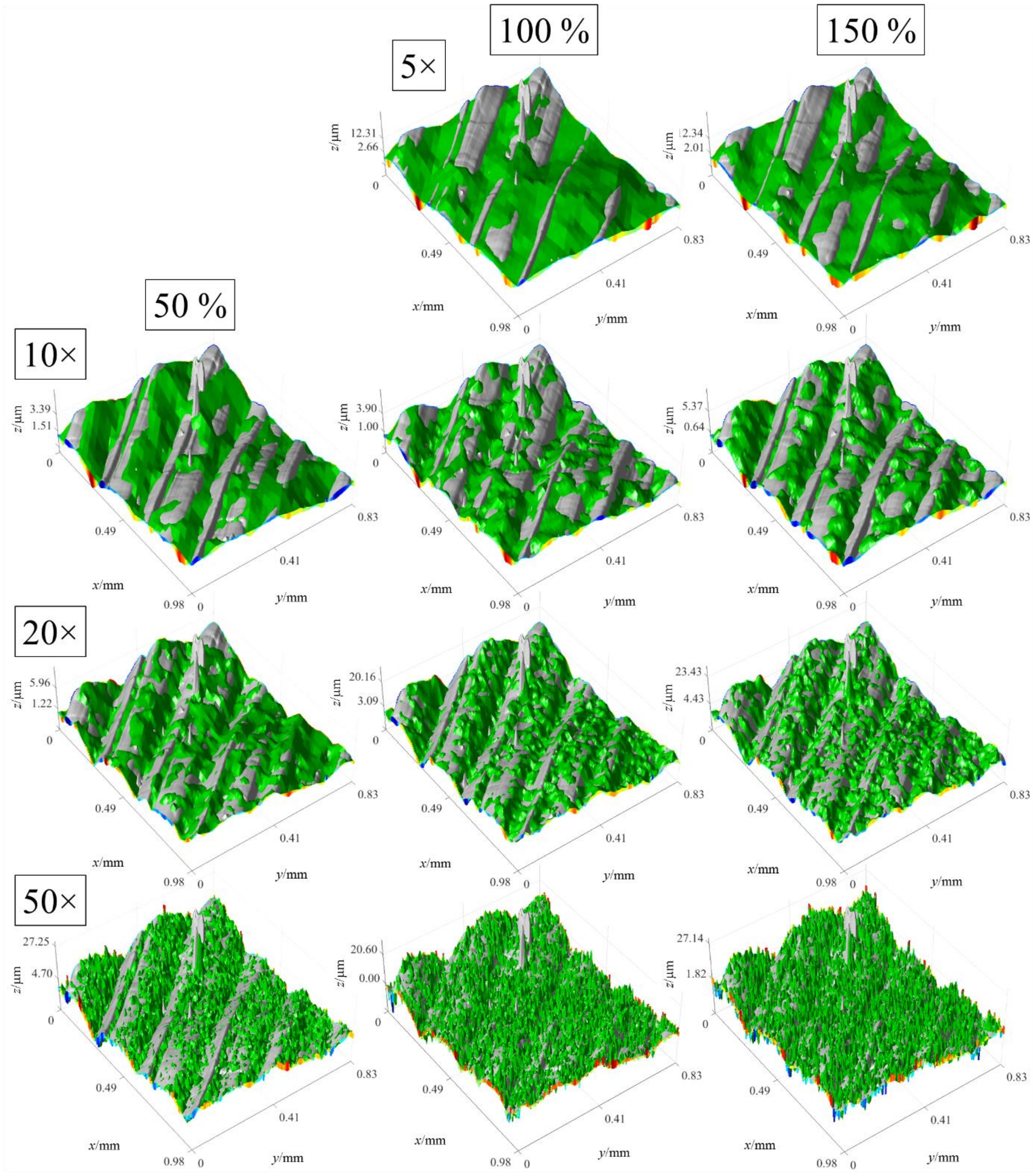

Figure 10. Local height differences (signed) computed between paired datasets, each pair comprised of one dataset for each XCT setup and a common CSI dataset. The 5×/50 % setup is omitted as the topographical detail of the reconstructed XCT surface was too deprived of topographical detail to allow accurate alignment to CSI data.

4. Discussion

4.1 XCT topography measurement

There is a large number of input parameters that affect XCT topography measurement, and two that are considered to be of greatest significance [9] have been examined in this work. Results show a general improvement in measurement quality when magnification is increased from 5× to 20×, i.e. reduced bias with respect to the CSI reference dataset and reduced repeatability error, but a significant decrease from 20× to 50×. This quality decrease is likely to be a result of an increase in the noise present in volumetric reconstructions, as shown in figure 3. Out-of-field-of-view artefacts [41] will contribute towards the increase in noise present in the 50× case, though noise also increased between the 5× and 20× setups. This noise increase is most likely as a result of a slight decrease in contrast with an increase in magnification, as the X-ray flux per unit volume through the sample increases with magnification [9]. Further noise increases may also result from the increasingly problematic effects of X-ray scatter [42] at higher magnifications. Nevertheless, further optimisation of all measurement setups is almost certainly possible, and may improve results.

For the purposes of this work, we have treated the XCT measurement system as an opaque system, and examined the effects of how altering certain input parameters to such an opaque system affects the outcome of a surface measurement. This decision was made as, while models of noise transmission are well studied in the literature [43–45], the transmission of noise in XCT measurement to a similar concept of noise in the terms of surface measurement is not yet understood, and represents significant future effort. There are of course many influencing factors on the measurement beyond the two variables examined here, including the X-ray source settings, focal spot size, detector characteristics and other reconstruction parameters, but these have been held constant for the purposes of this experiment. Investigation of these influence factors, all of which may have some influence on the image sharpness (and therefore the eventual extracted topography), represent significant avenues of future research.

Our results also provide insight into good practice in XCT surface measurement when considering the use of super- and sub-sampling of the reconstruction grid. Sub-sampling allows for small time savings in computation, but as shown here, significantly reduces the quality of the data when compared to reference measurements. Sub-sampling leads to distortions in determined surfaces and increases in CI width (see figure 6). Conversely, super-sampling of the reconstruction grid greatly increases processing time, while offering little to no improvement in the quality of the reconstructed topography. Although discrepancy ratios between statistical topography models of XCT and CSI measurements apparently decrease when the reconstruction grid is super-sampled, the decrease is clearly due to the widening of the CIs, which implies that there is not enough experimental evidence to determine whether or not datasets are discrepant. A simple observation of paired mean surfaces, and the associated mean unsigned distance between them, clearly shows that agreement has indeed decreased.

The data presented throughout this work help us to provide guidelines to successful surface measurement using XCT. For example, using a magnification of 5× clearly provides poor quality data by the metrics presented in this paper (see figures 7 and 8), and is likely insufficient for successful measurement of surfaces. Similarly, super- and sub-sampling of the reconstruction grid provides little benefit to the user. Improvements in data quality are generally provided by increasing magnification, but issues experienced at high magnification can also apparently cause issues that reduce the quality of the data. These issues, likely caused by the aforementioned out of field of view artefacts, decrease quality to the point where use of lower magnification may be beneficial to the user, despite the decrease in resolution. A case specific trade-off in magnification settings therefore exists, balancing the desire for the highest possible magnification with the baggage with which it comes. Because of this, we cannot recommend specific settings for successful surface measurement by XCT, but these findings should provide a basis by which XCT users may successfully conduct investigations of surfaces.

It is clear that many factors requiring investigation remain before XCT can become established as a common industrial method of surface measurement in industry. Particularly, more work is required to understand the uncertainty in such a measurement, and establishment of traceability for measurements of complex AM surfaces (by XCT or otherwise) is a difficult, open research question. Experiments should also be extended in future work to examine material and multi-material specific effects on XCT surface measurements; as material choice (and particularly the use of multi-material samples) have been previously shown to have significant effects on measurements [9]. However, the need is strong, in particular from the AM community, given the complex geometries commonly manufactured by AM processes and the likely presence of inaccessible or otherwise hard-to-reach surfaces.

In addition to the work presented in this paper, further assessment of how measurements are affected by the many unstudied variables factoring into XCT measurement is still required (for example, X-ray voltage and current, angular sampling, sample material). Such assessments will feed into good practice in industry, thereby facilitating increased adoption of AM technologies.

4.2 Comparison methodology

Very few of the results highlighted in this work could be captured by a simple comparison of ISO 25178-2 areal texture field parameters, which is the most common method in industry for performing comparative assessment of surface topographies. The application of our statistical topography modelling and comparison method (as established in our previous work [13,17] and further developed here), clearly shows that it is possible to investigate measurement differences, in terms of what causes them, how they appear on the surface, and where they are located.

Additional scientific merit of this study is, therefore, found in the proposition of a method to support reliable assessment of XCT sensitivity to control parameters, and as a tool for measurement process optimisation. The method does suffer some limitations, in that the quality of the statistical model is affected by alignment errors in the datasets. In this work, we have assumed the presence of minimal misalignment. However algorithmic global alignment is performed by applying the iterative closest point (ICP) method [38] in six degrees of freedom. The adopted approach is referred to as ‘global alignment’ as the optimisation takes into account the entirety of the datasets. However, one may wonder if, in the presence of significant differences between topographies, only the “less varying” regions should be considered as valid references for alignment. In addition, our current alignment method does not take into account the lesser reliability of points associated to higher repeatability error. Development of more advanced alignment solutions that account for both topographic differences and associated measurement errors is part of our ongoing work. Additionally, the method of statistical modelling used in this work can be refined by improving methods for computing local confidence intervals; for example by taking into account local spatial correlation between neighbouring surface points. Additional corrections to the statistical procedure for assessing local discrepancies may be adopted by introducing a correction factor for multiple comparisons (for example, Bonferroni [46]).

5. Conclusions

XCT measurement of areal surface topography is complex, and open to a wide array of influencing factors that may affect the eventual measurement results. However, XCT’s importance and potential in the domain of AM part quality inspection is undeniable. Our findings complement and improve upon the conclusions of previous work examining the use of XCT for areal topography measurement [7,13–15,17]. Specifically, in addition to showing that areal texture parameters vary significantly across setups, we have illustrated the details of how the reconstructed topography (from which the texture parameters are calculated) varies across setups. Geometric magnification has a stronger effect than sampling resolution in determining the quality and appearance of the topographic reconstruction. In particular, the magnification setup providing the best accuracy (compared to the CSI reference) was at 20× for the test case, while bias (again with respect to the CSI reference) decreased at smaller and larger magnifications.

Precision, indicated through the local repeatability error, consistently decreased with magnification. Modifying the sampling resolution (either by sub-sampling or super-sampling) has less pronounced effects; although generally, decreasing sampling resolution worsens metrological performance, while increasing it may lead to slight improvements. However, such improvements are unlikely to be justified in an industrial setting, as the time required to reconstruct, extract and process super-sampled surface topographies increases significantly with respect to the super-sampling ratio. At present, it is unclear as to what part of the presented results can be safely assumed as case-independent. What is clear, however, is that in XCT surface measurement, the optimal setup may not necessarily correspond to the highest magnification or highest reconstruction resolution, thus making the identification of an optimal measurement setup a non-trivial problem. Finally, we have demonstrated the importance and advantages of comparing measurement setups by means of statistical analysis of surface topographies reconstructed from measurement (as opposed to, or in addition to, the analysis of changes in texture parameter values). The amount of additional information that can be retrieved from the inspection of the actual topographic formations and how they vary as a consequence of measurement setup is invaluable when investigating the performance and behaviour of novel and partially unproven measurement technologies.

Acknowledgements

AT, IM and RKL. would like to thank EPSRC (Grants EP/M008983/1 and EP/L01534X/1) and 3TRPD Ltd. for funding this work. NS and RKL would also like to thank the EC for supporting this work through the grant FP7-PEOPLE-MC 624770 METROSURF. The authors would like to thank DigitalSurf for providing the MountainsMap software.

References

1. Gibson I, Rosen DW, Stucker B. Additive manufacturing technologies: 3D printing, rapid prototyping, and direct digital manufacturing. New York: Springer, 2014
2. Spierings AB, Starr TL, Wegener K. Fatigue performance of additive manufactured metallic parts. Rapid Prototyp J 2013;19;88–94
3. Xu Z, Hyde CJ, Thompson A, Leach RK, Maskery I, Tuck C, Clare AT. Staged thermomechanical testing of nickel superalloys produced by selective laser melting. Mater Des 2017;133;520–527
4. Gao W, Zhang Y, Ramanujan D, Ramani K, Chen Y, Williams CB, Wang CCL, Shin YC, Zhang S and Zavattieri PD. The status, challenges, and future of additive manufacturing in engineering. Comput Des 2015;69;65–89
5. UK Additive Manufacturing Steering Group. Additive manufacturing UK September 2016 strategy update. London: UK Additive Manufacturing Steering Group, 2016
6. Stavroulakis, PI, Leach, RK. Review of post-process optical form metrology for industrial-grade metal additive manufactured parts. Rev Sci Instrum 2016;87;41101
7. Thompson A, Senin N, Maskery I, Körner L, Lawes S, Leach RK. Internal surface measurement of metal powder bed fusion parts. Addit Manuf 2017;20;126-133
8. Thompson A, Maskery I, Leach, RK. X-ray computed tomography for additive manufacturing: a review. Meas Sci Technol 2016;27;72001
9. Camignato,S, Dewulf W, Leach, RK. (eds.) Industrial X-ray computed tomography. New York: Springer, 2017
10. Kerckhofs G, Pyka G, Moesen M, Van Bael S, Schrooten J, Wevers M. High-resolution microfocus X-ray computed tomography for 3D surface roughness measurements of additive manufactured porous materials. Adv Eng Mater 2013;15;153–158
11. Pyka G, Kerckhofs G, Braem A, Mattheys T, Schrooten J and Wevers M. Novel micro-ct based characterization tool for surface roughness measurements of porous structures. In: SkyScan User Meeting, Mechelen, Belgium, 2010;1–5
12. Thompson A, Körner L, Senin N, Lawes S Maskery I, Leach RK. Measurement of the internal surface texture of additively manufactured parts by X-ray computed tomography. In: Conf Industrial

Computed Tomography (iCT), Leuven, Belgium, 2017
13. Senin N, Thompson A, Leach, RK. Characterisation of the topography of metal additive surface features with different measurement technologies. Meas Sci Technol 2017;28;095003
14. Townsend A, Pagani L, Scott P, Blunt LA. Areal surface texture data extraction from X-ray computed tomography reconstructions of metal additively manufactured parts. Precis Eng 2017;48;254–264
15. Townsend A, Pagani L, Blunt L, Scott PJ, Jiang X. Factors affecting the accuracy of areal surface texture data extraction from X-ray CT. Ann. CIRP 2017;66;547–550
16. ISO 4287 Geometrical product specifications (GPS) -- surface texture: profile method -- terms, definitions and surface texture parameters. International organisation for standardization, 1997
17. Thompson A, Senin N, Giusca C, Leach RK. Topography of selectively laser melted surfaces: A comparison of different measurement methods. Ann. CIRP 2017;66;543–546
18. ISO 25178-606 Geometrical product specifications (GPS) -- surface texture: areal -- part 606: nominal characteristics of non-contact (focus variation) instruments. International organisation for standardization, 2015
19. Helmli F. Focus variation instruments. In: Leach, RK. editor: Optical measurement of surface topography. Berlin:Springer-Verlag, 2011;131–166
20. ISO 25178-2 Geometrical product specifications (GPS) -- surface texture: areal -- part 2: terms, definitions and surface texture parameters. International organisation for standardization, 2012
21. ISO/DIS 25178-607 Geometrical product specifications (GPS) -- surface texture: areal -- part 607: nominal characteristics of non-contact (confocal microscopy) instruments. International organisation for standardization, Under development
22. Artigas R. Imaging confocal microscopy. In: Leach, RK. editor: Optical measurement of surface topography. Berlin:Springer-Verlag, 2011;237–286
23. ISO 25178-604 Geometrical product specifications (GPS) -- surface texture: areal -- part 604: nominal characteristics of non-contact (coherence scanning interferometry) instruments. International organisation for standardization, 2013
24. de Groot P. Coherence scanning interferometry. In: Leach, RK. editor: Optical measurement of surface topography. Berlin:Springer-Verlag, 2011;187–208
25. VDI/VDE 2630 Part 1.1 Draft Computed tomography in dimensional measurement Fundamentals and definitions. VDI/VDE, 2014
26. Hsieh J. Image reconstruction. In: Computed tomography: principles, design, artifacts, and recent advances. SPIE Press:Bellingham, 2009;55–118
27. Hermanek P, Rathore JS, Aloisi V, Carmignato S. Principles of X-ray computed tomography. In Carmignato S, Dewulf W, Leach RK. editors: Industrial X-ray computed tomography. New York: Springer 2017;25–68
28. Bartscher M, Staude A, Ehrig K, Ramsey A. The Influence of data filtering on dimensional measurements with CT. In World Conf Non Destructive Testing, Durban, South Africa, 2012;16–20
29. NewView ™ 8300 Specifications. Zygo Corp 2017
30. Su R, Wang Y, Coupland J, Leach R. On tilt and curvature dependent errors and the calibration of coherence scanning interferometry. Opt Express 2017;25;3297–3310
31. Gomez C, Su R, Thompson A, DiSciacca J, Lawes S, Leach R. Optimisation of surface measurement for metal additive manufacturing using coherence scanning interferometry. Opt Eng 2017;56;111714
32. Volume Graphics. VGStudio MAX. 2017. Available at: http://www.volumegraphics.com/en/products/vgstudio-max.html Accessed: 27th November 2017
33. Kiekens K, Welkenhuyzen F, Tan Y, Bleys P, Voet A, Kruth J-P, Dewulf W. A test object with parallel grooves for calibration and accuracy assessment of industrial computed tomography (CT) metrology. Meas Sci Technol 2011;22;115502
34. Soille, P. Opening and closing. In: Morphological image analysis: principles and applications New

York: Springer-Verlag, 1999;105–137
35. Digital Surf. Mountains® surface imaging & metrology software. 2017 Available at: http://www.digitalsurf.com/en/mntkey.html. Accessed: 27th November 2017
36. MathWorks. MATLAB 2017a. 2017. Available at: https://uk.mathworks.com/products/matlab.html. Accessed: 27th November 2017
37. Gower JC. Generalized procrustes analysis. Psychometrika 1975;40;33–51
38. Besl PJ, McKay ND. A Method for Registration of 3D-Shapes. IEEE Trans Pattern Anal Mach Intel 1992;14;239–256
39. Leach RK, Haitjema H. Bandwidth characteristics and comparisons of surface texture measuring instruments. Meas Sci Technol 2010;21;32001
40. Gomez C, Su R, Thompson A, DiSciacca J, Lawes S, Leach RK. Optimisation of surface measurement for metal additive manufacturing using coherence scanning interferometry. Opt Eng 2017;56;111714
41. Leach RK. Fundamental principles of engineering nanometrology. Elsevier: Oxford, 2014
42. Hsieh J. Image artifacts: appearances, causes and correction. In: Computed tomography: principles, design, artifacts, and recent advances Bellingham: SPIE Press, 2009;207–300
43. Lifton J, Carmignato S. Simulating the influence of scatter and beam hardening in dimensional computed tomography. Meas Sci Technol 2017;28;104001
44. Hiller J, Hornberger P. Measurement accuracy in X-ray computed tomography metrology: toward a systematic analysis of interference effects in tomographic imaging. Precis Eng 2016;45;18–32
45. Illemann J, Bartscher M, Jusko O, Härtig F, Neuschaefer-Rube U, Wendt K. Procedure and reference standard to determine the structural resolution in coordinate metrology. Meas Sci Technol 2014;25;064015
46. Buzug TM. Computed tomogrpahy: from photon statistics to modern cone-beam CT. Springer: Berlin, 2008
47. Shaffer JP. Multiple hypothesis testing. Annu Rev Psychol 2995;46;561–584